H2020-FETFLAG-2018-2021

macQsimal

Miniature Atomic vapor-Cell Quantum devices for SensIng and Metrology AppLications

Deliverable D6.5

SERF-gyroscope feasibility report

WP6 – Miniature atomic gyroscope

Authors: Morgan Mitchell (ICFO)

Lead participant: ICFO

Delivery date: 30.03.2021

Dissemination level: Public

Deliverable Type: R (Document, Report)

macQsimal	Title	Deliverable Number
		D6.5
	SERF-gyroscope feasibility report	
Project Number		Version
820393		**Version 1.0**

Revision History

Author Name, Partner short name	Description	Date
Morgan Mitchell (ICFO)	Start of document	26.02.2021
Morgan Mitchell (ICFO)	Added descriptions of K – ^{3}He, Cs – ^{129}Xe, K – Rb – ^{21}Ne, and ^{87}Rb - ^{3}He - ^{129}Xe comagnetometer gyroscopes, feasibility assessments.	15.03.2021
Janine Riedrich-Möller (BOSCH) Tino Fuchs (BOSCH)	Review	19.03.2021
Morgan Mitchell (ICFO)	Revision based on BOSCH review	22.03.2021
Davide Grassani (CSEM) Sylvain Karlen (CSEM)	Review	26.03.2021
Morgan Mitchell (ICFO)	Final version (v1.0)	26.03.2021
Johannes Ripperger (accelCH)	Final formatting checks	30.03.2021

Abbreviations

AIG	Atom interferometer gyroscope
ARW	Angle Random Walk
ASG	Atomic spin gyroscope
CG	Comagnetometer gyroscope
CPT	Charge-Parity-Time
FIG	Fibre interferometer gyroscope
MEMS	Micro-electro-mechanical systems
NMR	Nuclear magnetic resonance
NMRG	Nuclear magnetic resonance gyroscope
RF	Radio frequency
RLG	Ring laser gyroscope
SD	Spin destruction
SE	Spin exchange
SERF	Spin exchange relaxation-free
VAARW	Volume-Adjusted Angle Random Walk

Contents

1 Overview / Executive summary

This document reviews the state of the art in SERF-regime comagnetometer gyroscopes (CGs) and the potential for their implementation with MEMS atomic vapor cells. This is relevant to macQsimal WP6 because CGs are a relatively new alternative to nuclear magnetic resonance gyroscopes (NMRGs), and in some contexts have shown better sensitivity and stability. CGs have been implemented with a variety of different atomic mixtures, including $K - {}^3He$, $Cs - {}^{129}Xe$, $K - Rb - {}^{21}Ne$, and ${}^{87}Rb - {}^3He - {}^{129}Xe$. We review the performance of these implementations and note challenges for their implementation in miniaturized sensors based on MEMS cells and other macQsimal technologies. The general conclusion is that while succeeding generations of laboratory CGs are improving in sensitivity and stability, these gains come less from an intrinsic superiority of the CG methods than from advances in laboratory technique. Furthermore, the more recent generations appear more difficult to miniaturize and in some cases the performance gains are only available at bandwidths not attractive for sensing applications such as inertial navigation.

2 Background and motivation

WP6 of macQsimal aims to develop rotation sensors (gyroscopes) built around miniaturized atomic vapor cells, as a technology for inertial sensing applications including inertial navigation for autonomous vehicles. Size, cost and sensitivity are all important for this application. Modern gyroscope technologies include, in order of increasing size, MEMS oscillators, optically pumped atomic spin gyroscopes (ASGs) that employ optically-pumped alkali vapors and noble gases, ring laser gyroscopes (RLGs), Sagnac fibre interferometer gyroscopes (FIGs), and atom interferometer gyroscopes (AIGs). AIGs, RLGs and FIGs have demonstrated sufficient sensitivity for inertial navigation applications, but are large and appear very difficult to miniaturize. MEMS oscillators can be very small, but do not have the required sensitivity or stability. In consequence, ASGs appear to be best suited for near-term practical application in inertial navigation.

One family of ASGs is the SERF-regime comagnetometer gyroscope. This uses alkali vapors in the spin-exchange-relaxation-free (SERF) regime of high density and low magnetic field, which can give very high alkali spin-coherence lifetimes and thus high sensitivity. In macQsimal WP4, SERF-regime vapors are being employed for magnetometry, using macQsimal MEMS cell technology. The potential for a cross-fertilization amongst these two WPs motivates the current study of SERF-regime CG methods, with a particular attention to the suitability for implementation with MEMS cell technology and for applications in inertial navigation.

3 Atomic gyroscope strategies

The class of ASG strategies known collectively as comagnetometer gyroscopes, share design elements with an ASG reported in a 2005 article "*Nuclear Spin Gyroscope Based on an Atomic Comagnetometer*" [1]. The term *comagnetometer* originates in fundamental physics studies and describes a sensor system in which two or more species, each of which has a magnetic response, are housed in the same volume and thus sense the same field. The term suggests a shortening of "co-located magnetometers". The comagnetometer strategy uses some form of cancellation, either of physical effects or of signals, to null the net sensitivity to magnetic noise, while retaining sensitivity to other effects. It should be noted that other atomic gyroscope strategies, e.g. NMRGs, can also use multiple species and differential measurement to cancel magnetic noise [2]. There is thus not a clear-cut distinction between comagnetometers and other ASGs. Indeed, there appears to be some convergence in technique between comagnetometers and dual-species NMRGs [3]. Nonetheless, the term is useful as it describes a family of related techniques with a common lineage.

In what follows, we review the state of the art in SERF-regime comagnetometer gyroscopes. For comparison, we describe also a more established strategy, the NMRG as implemented by Northrop Grumman. Qualitative and quantitative features of the different implementations are summarized in Table 1, organized by publication and by date (with the exception of the NMRG reference).

Table 1: Literature on implemented SERF-regime atomic gyroscopes. The first entry, Walker and Larsen 2016, describes the NMR gyroscope of Northrop Grumman, as a point of reference. Some entries indicate calculated ultimate sensitivities, i.e., predictions of sensitivity if all technical noise sources could be eliminated. These are orders of magnitude beyond current sensitivities suggesting that, in principle, any of these technologies could be highly sensitive. "n.g." indicates that a value was not given in the cited work.

Reference	Year	Alkali	Noble gas	Other gas	Temperature °C	Active volume cm^3	ARW rad s^{-1}Hz$^{-1/2}$	VAARW rad s^{-1}Hz$^{-1/2}$cm$^{3/2}$	Bias stability deg h^{-1}
Walker and Larsen [2]	2016	Rb	^{131}Xe	N$_2$	> 120	8×10^{-3}	1.4×10^{-6}	1×10^{-7}	2×10^{-2}
Kornack et al. [1]	2005	K	7 amg ^{3}He	20 Torr N$_2$	170	0.5	5×10^{-7}	2.5×10^{-7}	n.g.
Kornack [4]	2005	K	7 amg ^{3}He	20 Torr N$_2$	170	3	2×10^{-10} (calculated ultimate sensitivity)	6×10^{-10} (calculated ultimate sensitivity)	< 0.1
Smiciklas et al. [5]	2011	K, ^{87}Rb	2 amg ^{21}Ne	30 Torr N$_2$	200	1.4	n.g.	n.g.	n.g.
Fang and Qin [6]	2012	Cs	^{129}Xe	n.g.	n.g.	n.g.	1.2×10^{-6}	n.g.	n.g.
Fang et al. [7]	2013	Cs	20 Torr ^{129}Xe	700 Torr N$_2$	110	8	1.7×10^{-5}	1.4×10^{-4}	3.25
Fang et al. [8]	2016	K, Rb	2.7 amg ^{21}Ne	31 Torr N$_2$	185	1.4	4.6×10^{-7} (estimated from mag. sensitivity)	6.4×10^{-7}	n.g.
Dong and Gao [9]	2016	as in [1]	as in [1]	as in [1]	as in [1]			5×10^{-11} (calculated ultimate sensitivity)	
Dong and Gao [9]	2016	Cs	1 atm Xe	n.g.	n.g.			8×10^{-11} (calculated ultimate sensitivity)	
Chen et al. [10]	2016	K, Rb (nat.)	3 atm ^{21}Ne	40 Torr N$_2$	185	1.4	2.1×10^{-8} (at 5 Hz, estimated from mag. sensitivity)	3.0×10^{-7} (at 5 Hz, estimated from mag. sensitivity)	n.g.
Li et al. [11]	2016	K, Rb (nat.)	2.3 amg ^{21}Ne	50 Torr N$_2$	180	0.5	n.g.	n.g.	1×10^{-1}
Li et al. [12]	2017	K, Rb (nat.)	2.1 amg ^{21}Ne	20 Torr N$_2$	185	0.5	n.g.	n.g.	2×10^{-2}
Limes et al. [3]	2018	^{87}Rb	9.3 atm ^{3}He + 2.9 Torr ^{129}Xe	40 Torr N$_2$	110-120	0.5	3×10^{-6}	1.5×10^{-6}	$\leq 9 \times 10^{-3}$
Fan et al. [13,14]	2019	K, Rb (nat.)	1100 Torr ^{21}Ne	50 Torr N$_2$	160-200	0.5	1×10^{-7} (at 1 Hz)	5×10^{-8} (at 1 Hz)	5×10^{-4}
Shi [15]	2020	^{87}Rb	20 Torr ^{129}Xe	700 Torr N$_2$	160		n.g.	n.g.	n.g.

3.1 Sensitivity and stability figures of merit

In the CG literature, the most commonly given measure of sensitivity is angle random walk (ARW), typically given in deg $h^{-1/2}$ or, as we will use here, rad $s^{-1}Hz^{-1/2}$. As miniaturization is of interest, and some experiments use larger cells, we also give the volume-adjusted angle random walk (VAARW), defined as the ARW times the square root of the volume of the sensor, with units rad $s^{-1}Hz^{-1/2}cm^{3/2}$. ARW and VAARW describe the short-term sensitivity or short term stability and does not characterize the stability on long time scales. Most sensors in the literature show significant 1/f noise at relevant frequencies, e.g., 1 Hz. To quantify this, a relevant figure of merit is the drift or bias stability, typically given in deg h^{-1}. A few experimental reports give Allan deviations for their gyroscope signals [2,3,7]. We have included these as graphs in the corresponding sections, but not in Table 1, due to the inherently multi-dimensional nature of this characterization.

4 NMR Gyroscope
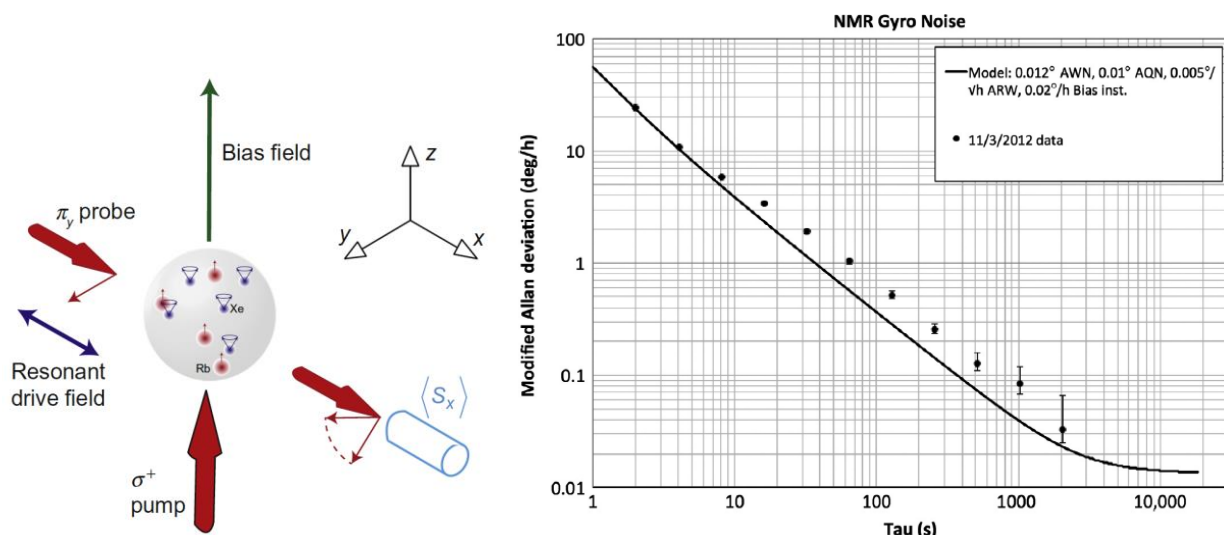
Figure 1: NMR gyroscope operation and stability (figures from [2]). **Left**: *a simple NMR gyro scheme. Rb atoms are spin polarized by the pump laser, transfer angular momentum to Xe nuclei via collisions, and detect the magnetic field produced by the precessing Xe nuclei by causing a Faraday rotation of the polarization of the probe laser. The polarized Xe nuclei are driven to precess by the resonant oscillating drive field. The phase shift between the drive field and the oscillation of the nuclear precession about the bias field direction changes when the apparatus rotates about the bias field direction.* **Right**: *Allan deviation of gyroscope stability.*

The most intensively developed ASG strategy is the NMRG [2], illustrated in Figure 1, which has been developed in industrial laboratories since the late 1970s [16]. In NMRG, the vapor cell will contain an alkali species and a noble gas, which we will assume are Rb and Xe, along with buffer gas and possibly other components to reduce relaxation due to wall collisions. In the presence of a constant bias magnetic field, the Xe is spin-polarized along the field by spin-exchange with the Rb, which itself is polarized in this direction by optical pumping. A Xe-resonant RF field can then be used to tip the Xe polarization, which in turn tips the Rb polarization, an effect that can be detected by e.g. Faraday rotation with off-resonance light. The resonant nature of this signal allows the *lab frame* Xe Larmor frequency to be determined, which reveals the rotation rate of the apparatus about the applied field, provided the field strength is known.

A well-developed NMRG implementation has been presented by Northrop-Grumman [3], which reports an ARW of 1.4×10^{-6} rad $s^{-1}Hz^{-1/2}$, and a bias stability of 2×10^{-2} deg h^{-1}.

5   SERF-regime comagnetometer gyroscopes
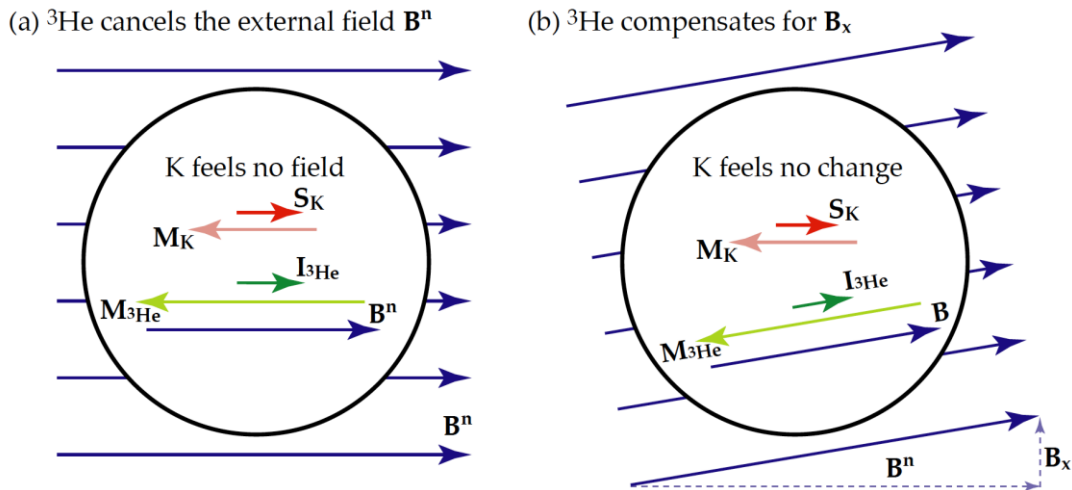
Figure 2: Illustration of the $K - {}^3He$ comagnetometer gyroscope (from [4]). a) shows the equilibrium condition, in which the alkali (K in the figure) spin polarization S_K is optically pumped along the z direction (to the right in the figure), producing a spin polarization I_{He} in the noble gas (He in the figure) also along z. The effective magnetic field experienced by the alkali includes the external field B^n and the effective field M_{He} produced by the noble gas nuclei both through their dipole moment and through the imaginary part of the alkali-noble spin-exchange collision cross section. The strength B of the field is chosen such that B and M_{He} cancel, and the alkali spin experiences no net field. b) shows the result of a change in magnetic field direction from this equilibrium condition: the noble gas spin polarization adiabatically follows the field, and the alkali still feels no net field. In this way the setup automatically cancels the effect of an external field. In contrast, a rotation of the apparatus implies (in the frame of the apparatus) both a change in the external magnetic field and an additional inertial torque on I_{He}. These effects do not cancel, and the alkali spin rotates relative to the apparatus to give a finite signal proportional to Ω_y, the rotation rate.

The SERF-regime CG shares many elements with the NMRG. A noble gas is used as the rotation sensor, and an alkali is used both for optical pumping of the noble gas and for readout. The mechanism is described and illustrated in Figure 2.

The most sensitive optically-pumped magnetometers [17] operate in the SERF (spin-exchange-relaxation free) regime [18] [19], which occurs in alkali vapors at high density and low field strength. The effect allows simultaneous high alkali density and long coherence times, with a consequent boost in sensitivity. A SERF-regime comagnetometer gyroscope takes advantage of this by working with high alkali density and low effective field for the alkali.

5.1   K – ³He SERF comagnetometer gyroscope

The first comagnetometer gyroscope was demonstrated by Kornack et al. [1] in 2005, based on a previous analysis of the spin-exchange physics of alkali-noble gas mixtures [20]. The comagnetometer employed a mixture of K and ^{3}He and achieved an ARW of $5 \times 10^{-7} \text{rad s}^{-1}\text{Hz}^{-1/2}$, somewhat better than the Northrop-Grumman NMRG. At the same time, its bias stability of $10^{-1} \, deg \, h^{-1}$ is considerably worse. Despite Kornack et al. 2005 being a widely cited work, the K-^{3}He mixture has not been the subject of much experimental study afterward. A notable work with this method is Fang et al. 2016 [8], which reports an ARW of $4.6 \times 10^{-7} \text{rad s}^{-1}\text{Hz}^{-1/2}$, slightly better than the original 2005 work.

5.1.1   Observations on the feasibility of K – ³He CG miniaturization

The K-^{3}He comagnetometer presents a few technical inconveniences relative to the NMRG. For one, the working temperature is higher, due to the low vapor pressure of K. Also the He pressure, up to 7 amg in

the work by Kornack et al., is high. The relative complexity of the physics, which relies upon a multi-step interaction among the field, alkali, and noble gas spins, is also a possible deterrent to pursuing this strategy for applications. At present, the ARW of this strategy is slightly better that the Northrop Grumman NMRG, but uses a larger cell volume. When adjusted for volume, i.e., using VAARW, neither the sensitivity nor the bias stability surpasses the Northrop Grumman NMRG. It is of course possible that a CG strategy would improve with further development, but it is also possible that miniaturization would increase relevant noise or drift levels, e.g., in the magnetic environment.
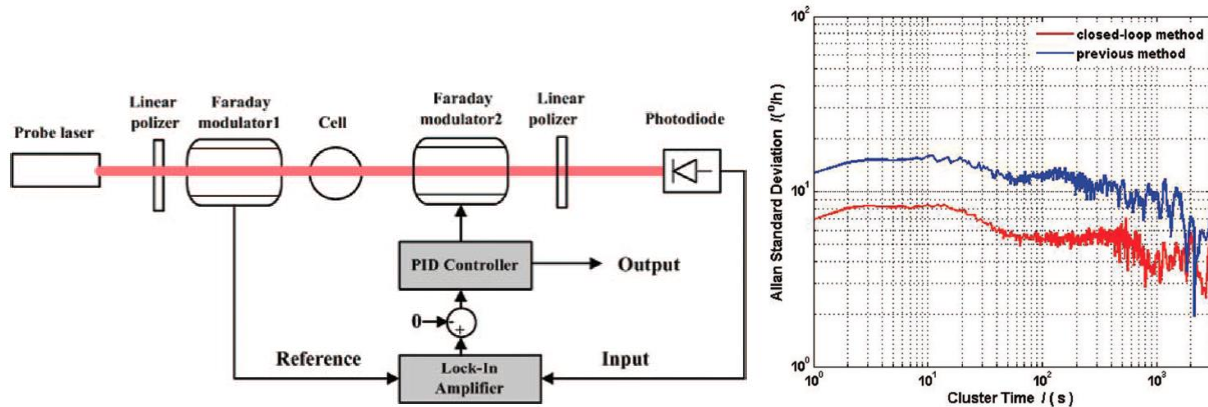
Figure 3: *Illustration of the Cs – ^{129}Xe comagnetometer gyroscope (from [7]).* **Left**: *schematic of the experimental setup.* **Right**: *Allan deviation.*

5.2   Cs – ^{129}Xe SERF comagnetometer gyroscope

This CG approach was introduced by Fang et al. in 2013 [7]. The Cs – ^{129}Xe CG is able to work at lower working temperatures and lower overall pressures. It has been studied in only a few publications.

5.2.1   Observations on the feasibility of Cs – ^{129}Xe CG miniaturization

The Cs – ^{129}Xe comagnetometer suffers from a basic drawback in the collision physics: the alkali spin relaxation rate is much faster in this mixture than in others, due to SD collisions in which CsXe Van der Waals molecules are formed [21]. This perhaps accounts for the relatively poor ARW of 1.7×10^{-5} rad s^{-1}Hz$^{-1/2}$ in the best-documented example of this strategy [8].
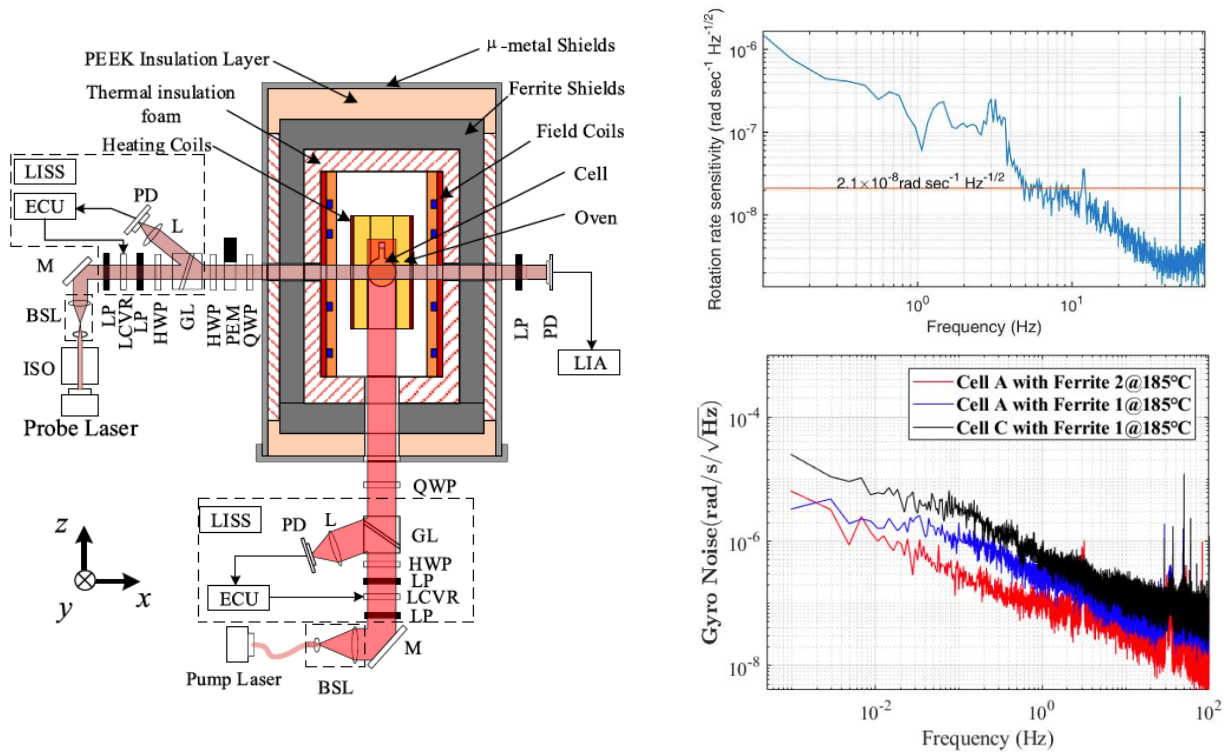
Figure 4: *Illustration of the K – Rb – ^{21}Ne comagnetometer.* **Left**: *Schematic of the co-magnetometer (from [14]). ISO: isolator, BSL: beam shaping lenses, M: reflection mirror, LP: linear polarizer, LCVR: liquid crystal variable retarder, HWP: half wave plate, GL: Glan-Prism, QWP: quarter wave plate, L: lens, PD: photodiode, PEM: photo-elastic modulator, LIA: lock-in amplifier, ECU: electronic control unit, LISS: laser intensity stabilization system. The LISS is used to guarantee the long-term stability of the intensity of the pump and probe lasers. A LISS mainly compromises of two crossed LPs, a LCVR, a HWP, a GL, a PD and an ECU. The output laser intensity of the LISS is monitored by the PD, which detects the intensity of a small portion of laser split by the GL. The PD signal is fed into the ECU. The ECU compares the current laser intensity with the set-point value and changes the driving voltage applied to the LCVR to change the output laser intensity.* **Top right**: *Sensitivity (from [10]).* **Bottom right**: *Sensitivity (from [13]).*

5.3 K – Rb – ^{21}Ne SERF comagnetometer gyroscope

This strategy was introduced by Smiciklas et al. [5] in 2011 in the context of a fundamental physics test. The first uses as a gyroscope were by the group of Jiancheng Fang in 2016 [11,22–24]. The use of ^{21}Ne rather than ^{3}He as a noble gas provides an immediate advantage; the gyromagnetic ratio of ^{21}Ne is an order of magnitude smaller than that of ^{3}He, making it less sensitive to magnetic noise and drift. ^{21}Ne is a spin-3/2 nucleus, and thus has a quadrupole moment, which causes spin relaxation much faster than ^{3}He. To overcome this, the strategy uses Rb for SE pumping of the ^{21}Ne, and to permit very high Rb densities, uses optically-pumped K to polarize the Rb by SE.

Since its initial use as a gyroscope, the method has been the subject of relatively intense study compared to other methods [11,13,14,22,23,25], with the best reported performance [13,14] giving ARW of 1×10^{-7} rad s^{-1}Hz$^{-1/2}$ at 1 Hz, corresponding to VAARW of 5×10^{-8} rad s^{-1}Hz$^{-1/2}$cm$^{-3/2}$ (also at 1 Hz) and bias stability of 5×10^{-4} deg h^{-1}. The VAARW is slightly better than the Northrop-Grumman NMRG, while the bias stability is much better.

5.3.1 Observations on the feasibility of K − Rb − ^{21}Ne CG miniaturization

The physical conditions for this strategy: about 1.5-3 atm of noble gas plus tens of Torr of N$_2$ for quenching, up to 200 °C temperature, are somewhat more demanding than typical NMRG, but are probably not prohibitive. Spherical cells are employed, because 1) the quadrupole moment of the ^{21}Ne nucleus makes it sensitive to the wall orientation in collisions and 2) the high density of the spin-polarized Rb vapor implies a significant Rb-induced magnetic field that would be inhomogeneous if contained in a cell with other geometry. The hybrid pumping technique requires a high optical power (a 1W tapered amplifier system was used in [22]).

The relatively fast SE time scale for K − Rb − ^{21}Ne pumping and relaxation relative to K − ^{3}He is in some sense a practical advantage: the devices require only tens of seconds, rather than hours, to develop an initial noble gas polarization.

The complexity of the physics is still higher than that of the K − ^{3}He comagnetometer strategy: there are two alkalis and quadrupolar interactions play a significant role. At the same time, the use of high-density Rb to polarize the ^{21}Ne implies a strong effective magnetic field produced by the Rb on the ^{21}Ne, of order 100 nT. This effective field is useful in that it reduces the sensitivity of the system to external fields [8], but also makes the optical pumping physics a significant source of noise and drifts. In parallel to this, the effective field experienced by the Rb due to the ^{21}Ne spins is still larger, $\sim 500\ nT$. The effect of having two significant effective fields is that the system is compensated (i.e., magnetically insensitive) at a finite net field for each species. As a consequence, the Rb spins cannot be maintained fully in the SERF regime, and experience significant SE relaxation.

It should be noted that the level of technology applied in the more recent publications on the K − Rb − ^{21}Ne system is quite high, including five-layer (four mu-metal layers plus ferrite) magnetic shielding, "noise eater" laser power stabilization, a vacuum of ~1 mTorr for thermal insulation, water-cooling of magnetic shields, and a rotation platform plus solar tracking system to maintain the sensitive access direction [22], which is described as necessary to cancel the contributions of laser power fluctuations. This level of effort is appropriate when building a comagnetometer for fundamental physics studies, but appears prohibitive for inertial navigation applications.
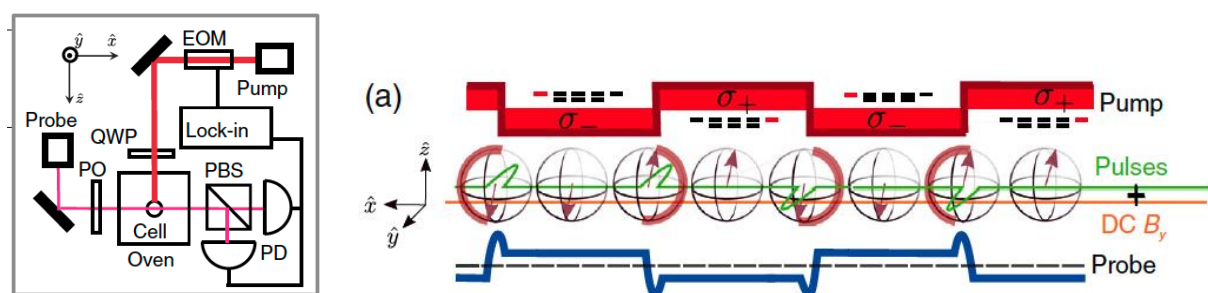
Figure 5: *Illustration of the ^{87}Rb - ^{3}He - ^{129}Xe comagnetometer (from [3]). **Left:** schematic diagram of the setup. **Right:** pulse sequence for readout of the effective magnetic field produced by the noble gas components.*
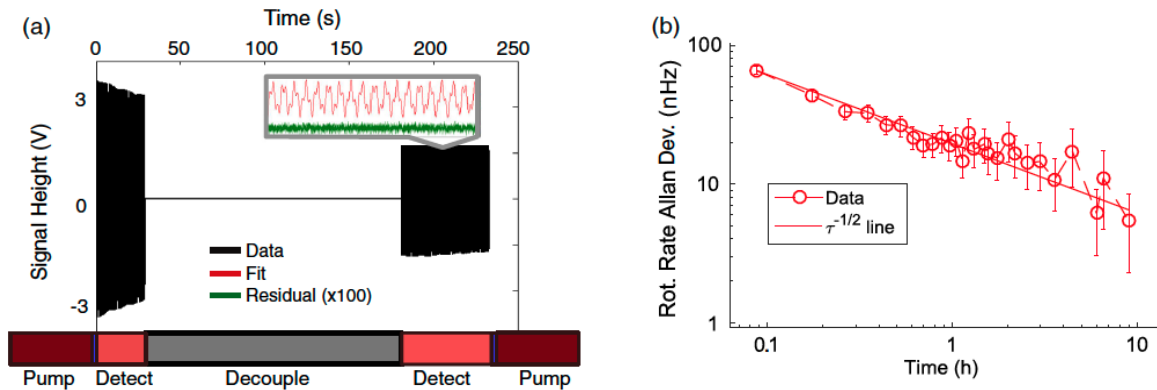
Figure 6: *^{87}Rb - ^3He - ^{129}Xe comagnetometer sequence and stability (from [3]). a) shows the temporal sequence. b) shows the Allan deviation.*

5.4 ^{87}Rb - ^{3}He - ^{129}Xe SERF comagnetometer gyroscope

This strategy, illustrated in Figure 5 and Figure 6, was introduced by Limes et al. [3] in 2018, in the context of fundamental physics experiments. The approach uses two noble gas species in a single spherical cell volume. The two species have differing response to magnetic fields, while experiencing rotation in the same way. When each species is used as a spin-precession magnetometer, a differential measurement of the apparent magnetic field is then sensitive to rotation but insensitive to magnetic fluctuations. ^{87}Rb is used to spin-polarize the noble gas species and for readout. This ordinarily would cause large systematic shifts, because of the effective field of the ^{87}Rb, as discussed in the previous section. To counter this, the Rb is put through a series of operations (pi pulses to reverse the spin precession and optical pumping alternately along and against the magnetic field) such that the net effective field experienced by the noble gas species is greatly reduced during the free-precession time. The achieved sensitivity (ARW of 3×10^{-6} rad s^{-1}Hz$^{-1/2}$and VAARW of 1.5×10^{-6} rad s^{-1}Hz$^{-1/2}$cm$^{3/2}$) are still somewhat worse than the Northrop Grumman NMRG, while the stability ($\leq 9 \times 10^{-3}$ deg h^{-1}) is better by at least a factor of two.

5.4.1   Observations on the feasibility of ^{87}Rb - ^{3}He - ^{129}Xe CG miniaturization

The strategy uses an easily achievable temperature of about 110 °C. The pressure of 9 atm ^{3}He is quite high. The strategy employs spherical cell volumes, for the reasons given in 5.3.1 above. The required optical power level is not specified, but presumably is not low, given the need to rapidly switch the Rb polarization by optical pumping. The process also requires a train of RF pulses of 1-2 Ampere in amplitude and 1.5-3 µs in duration.

A more essential impediment presents itself, however: To avoid contamination of the ^{3}He and ^{129}Xe precession signal by spin-exchange with ^{87}Rb, the comagnetometer is operated as a Ramsey interferometer, with a long free-precession time between excitation and read-out. During this "dark time", which is 150 s in the Limes et al. implementation, the ^{87}Rb has been depolarized and the optical pumping is off. No signal is acquired during this time; rather, the net rotation angle is recovered at the end of the dark time. There are also roughly 90 seconds of measurement time at the beginning and end of the Ramsey sequence, giving a total of 240 seconds between measurements of the rotation angle. The bandwidth of such a measurement is then roughly 1 point per four minutes, a number better suited to fundamental physics than to inertial navigation. Increasing the bandwidth by reducing the preparation,

free-evolution, and readout time would reduce the sensitivity and possibly place greater demands on the optical and magnetic control systems to rapidly implement the required complex pulse sequence.

6   Comparison of ultimate sensitivity of NMRG and SERF CG

A theoretical work by Dong and Gao published in three versions on arXiv [9], with the final version published in IEEE Advances [26], presents a common model NMRG and SERF comagnetometer response. The earliest arXiv version argues that the ultimate sensitivity of the $K - {}^3He$ SERF comagnetometer and a Xe based NMRG are similar. This claim does not appear in the later versions.

For a few specific cases the ultimate sensitivity, i.e. the sensitivity that could be achieved if all technical noise and drifts were eliminated, has been calculated [4,9]. These find the ultimate sensitivity is far better than the demonstrated performance to date. The advantage of one strategy over another will thus be determined by how well the strategy can decouple the rotation signal from achievable levels of noise and drift in a variety of parameters including magnetic field, temperature, and laser power.

7   Conclusions

We have reviewed the state of the art in comagnetometer gyroscopes, with a particular attention to the possibility of implementing them with the miniaturization technologies developed and employed in macQsimal. The broad picture is that comagnetometer gyroscopes are advancing in sensitivity and stability, becoming competitive with NMRG technologies that have been the subject of longer development efforts. At the same time, the comagnetometer techniques achieve this performance in laboratory implementations that appear difficult to miniaturize without sacrificing performance. The most advanced comagnetometer solutions, moreover, are tailored to applications in fundamental physics. They embody trade-offs, e.g., by sacrificing bandwidth to increase sensitivity, that are appropriate for that application but not for sensing applications such as inertial navigation.

8   References

[1] T. W. Kornack, R. K. Ghosh, and M. V. Romalis, *Nuclear Spin Gyroscope Based on an Atomic Comagnetometer*, Physical Review Letters **95**, 230801 (2005).

[2] T. G. Walker and M. S. Larsen, *Chapter Eight - Spin-Exchange-Pumped NMR Gyros*, in *Advances In Atomic, Molecular, and Optical Physics*, edited by E. Arimondo, C. C. Lin, and S. F. Yelin, Vol. 65 (Academic Press, 2016), pp. 373–401.

[3] M. E. Limes, D. Sheng, and M. V. Romalis, *3He-129Xe Comagnetometery Using 87Rb Detection and Decoupling*, Phys. Rev. Lett. **120**, 033401 (2018).

[4] T. Kornack, A Test of CPT and Lorentz Symmetry Using a K-3He Co-Magnetometer, PhD Thesis, Princeton, 2005.

[5] M. Smiciklas, J. M. Brown, L. W. Cheuk, S. J. Smullin, and M. V. Romalis, *New Test of Local Lorentz Invariance Using a 21Ne-Rb-K Comagnetometer*, Physical Review Letters **107**, 171604 (2011).

[6] J. Fang and J. Qin, *Advances in Atomic Gyroscopes: A View from Inertial Navigation Applications*, Sensors **12**, 5 (2012).

[7] J. Fang, S. Wan, J. Qin, C. Zhang, W. Quan, H. Yuan, and H. Dong, *A Novel Cs-129Xe Atomic Spin Gyroscope with Closed-Loop Faraday Modulation*, Review of Scientific Instruments **84**, 083108 (2013).

[8] J. Fang, Y. Chen, S. Zou, X. Liu, Z. Hu, W. Quan, H. Yuan, and M. Ding, *Low Frequency Magnetic Field Suppression in an Atomic Spin Co-Magnetometer with a Large Electron Magnetic Field*, Journal of Physics B: Atomic, Molecular and Optical Physics **49**, 065006 (2016).

[9] H. Dong and Y. Gao, *Direct Comparison of Nuclear-Spin-Gyroscope Schemes*, ArXiv:1606.08924v1 [Physics, Physics:Quant-Ph] (2016).

[10] Y. Chen, W. Quan, S. Zou, Y. Lu, L. Duan, Y. Li, H. Zhang, M. Ding, and J. Fang, *Spin Exchange Broadening of Magnetic Resonance Lines in a High-Sensitivity Rotating K-Rb-21Ne Co-Magnetometer*, Scientific Reports **6**, 36547 (2016).

[11] R. Li, W. Fan, L. Jiang, L. Duan, W. Quan, and J. Fang, *Rotation Sensing Using a K-Rb-21Ne Comagnetometer*, Phys. Rev. A **94**, 032109 (2016).

[12] R. Li, W. Quan, W. Fan, L. Xing, and J. Fang, *Influence of Magnetic Fields on the Bias Stability of Atomic Gyroscope Operated in Spin-Exchange Relaxation-Free Regime*, Sensors and Actuators A: Physical **266**, 130 (2017).

[13] W. Fan, W. Quan, F. Liu, L. Xing, and G. Liu, *Suppression of the Bias Error Induced by Magnetic Noise in a Spin-Exchange Relaxation-Free Gyroscope*, IEEE Sensors Journal **19**, 9712 (2019).

[14] W. Fan, W. Quan, W. Zhang, L. Xing, and G. Liu, *Analysis on the Magnetic Field Response for Nuclear Spin Co-Magnetometer Operated in Spin-Exchange Relaxation-Free Regime*, IEEE Access **7**, 28574 (2019).

[15] M. Shi, *Investigation on Magnetic Field Response of a 87Rb-129Xe Atomic Spin Comagnetometer*, Opt. Express **28**, 32033 (2020).

[16] B. C. Grover, E. Kanegsberg, J. C. Mark, and R. L. Meyer, *Nuclear Magnetic Resonance Gyro*, US4157495A (1979).

[17] D. Budker and M. Romalis, *Optical Magnetometry*, Nature Phys. **3**, 227 (2007).

[18] J. C. Allred, R. N. Lyman, T. W. Kornack, and M. V. Romalis, *High-Sensitivity Atomic Magnetometer Unaffected by Spin-Exchange Relaxation*, Physical Review Letters **89**, 130801 (2002).

[19] I. Kominis, T. Kornack, J. Allred, and M. Romalis, *A Subfemtotesla Multichannel Atomic Magnetometer*, Nature **422**, 596 (2003).

[20] T. W. Kornack and M. V. Romalis, *Dynamics of Two Overlapping Spin Ensembles Interacting by Spin Exchange*, Phys. Rev. Lett. **89**, 253002 (2002).

[21] X. Zeng, Z. Wu, T. Call, E. Miron, D. Schreiber, and W. Happer, *Experimental Determination of the Rate Constants for Spin Exchange between Optically Pumped K, Rb, and Cs Atoms and 129Xe Nuclei in Alkali-Metal--Noble-Gas van Der Waals Molecules*, Phys. Rev. A **31**, 260 (1985).

[22] Y. Chen, W. Quan, S. Zou, Y. Lu, L. Duan, Y. Li, H. Zhang, M. Ding, and J. Fang, *Spin Exchange Broadening of Magnetic Resonance Lines in a High-Sensitivity Rotating K-Rb- 21 Ne Co-Magnetometer*, Scientific Reports **6**, 1 (2016).

[23] J. Fang, Y. Chen, Y. Lu, W. Quan, and S. Zou, *Dynamics of Rb and 21Ne Spin Ensembles Interacting by Spin Exchange with a High Rb Magnetic Field*, Journal of Physics B: Atomic, Molecular and Optical Physics **49**, 135002 (2016).

[24] J. Fang, Y. Chen, S. Zou, X. Liu, Z. Hu, W. Quan, H. Yuan, and M. Ding, *Low Frequency Magnetic Field Suppression in an Atomic Spin Co-Magnetometer with a Large Electron Magnetic Field*, Journal of Physics B: Atomic, Molecular and Optical Physics **49**, 065006 (2016).

[25] Y. Yang, D. Chen, W. Jin, W. Quan, F. Liu, and J. Fang, *Investigation on Rotation Response of Spin-Exchange Relaxation-Free Atomic Spin Gyroscope*, IEEE Access **7**, 148176 (2019).

[26] H. Dong and Y. Gao, *Comparison of Compensation Mechanism Between an NMR Gyroscope and an SERF Gyroscope*, IEEE Sensors Journal **17**, 4052 (2017).